A FINITE-VOLUME MODEL FOR THE SIMULATION OF THE HOT STRIP ROLLING PROCESS

Luciano Pessanha Moreira
Universidade Federal Fluminense, Av. dos Trabalhadores 420 CEP 27 255-125 Volta Redonda RJ Brazil
luciano.moreira@metal.eeimvr.uff.br

José Adilson de Castro
Universidade Federal Fluminense, Av. dos Trabalhadores 420 CEP 27 255-125 Volta Redonda RJ Brazil
adilson@metal.eeimvr.uff.br

Ronaldo Barbosa
Universidade Federal de Minas Gerais, R. Espírito Santo 35 - Sala 206- Centro CEP30 160-030- Belo Horizonte, MG Brazil
rbarbosa@demet.ufmg.br

Alexandre José da Silva
Universidade Federal Fluminense, Av. dos Trabalhadores 420 CEP 27 255-125 Volta Redonda RJ Brazil
ajs@metal.eeimvr.uff.br

Abstract. *A mathematical model for the hot rolling process is proposed in an attempt to determine useful parameters in the hot rolling operation such as the rolling loads, temperatures and the microstructure evolution. The model predicts the local behavior of important variables in the thermomechanical processing, namely, the effective strain-rate, the stress and strain states. The hot rolling process is described by means of the transport equations of energy, mass and momentum in the steady state flow. A non-Newtonian formulation and an Eulerian description are adopted along with the Finite Volume (FV) method. In this formulation, the strain and strain-rate fields are firstly obtained from the pressure and velocities fields solutions and provide with the temperature fields and, a constitutive equation, the apparent viscosity of the material allowing, in this way, to determine the stresses and, therefore, the rolling load. The material constitutive equation takes into account the microstructural phenomena associated with the hot rolling process, i.e., work-hardening, recovery and recrystallisation. The numerical predictions have been compared with the measured rolling loads and temperatures for the finishing mill of a low carbon steel. It is shown that the rolling load predictions depend mainly upon the material constitutive behavior which, in turn, should describe the effects of strain, strain-rate and temperature with its dependence upon the microstructural evolution during the hot rolling process. The adopted roll-gap heat transfer coefficient has also revealed to have a great effect upon the predicted rolling loads.*

Keywords*: transport equations, finite volume method, numerical simulation, hot rolling*

1. Introduction

The mathematical modeling of the hot rolling process is an extremely hard task because of the deformation coupled to the temperature, the microstructure phenomena as well as the range of temperatures, strains and strain-rates which, in turn, cannot be well reproduced or even monitored under laboratory conditions. The mathematical models for describing the hot rolling process in the literature can vary from roll force and torque models based upon the works of Orowan and *[Proc. Inst. of Mech. Engrs. 150 (1943) 140]* and Sims *[Proc. Inst. of Mech. Engrs. 168 (1954) 191]* up to stand alone and integrated Finite Element (FE) models, e.g., Mukhopadhyay et al. *[Mat. Sci. and Technology 20 (2004) 1123]* and Zhou *[J. of Mat. Proc. Technology 134 (2003) 338]*. In bulk metal forming processes such as the hot rolling, the elastic strains are usually very small in comparison to the high plastic strain levels and then can be neglected. This assumption makes possible to consider the deformation process by means of a flow formulation together with the Finite Volume (FV) method which is very attractive essentially from the standpoint of the computation time cost. This approach is adopted in the present work where the basic constitutive equations are first presented in order to establish the analogy between the deformation of a solid and the incompressible flow of a non-Newtonian fluid. Afterwards, the transport equations are detailed for the general three-dimensional case in an Eulerian reference frame, namely, the balance laws for conservation of energy, momentum and mass respectively. The microstructural changes taking place during the hot rolling process are implemented in the proposed FV model. This is firstly accomplished by means of a flow-stress constitutive equation describing the restoration mechanisms due to the dynamic recovery and dynamic recrystallization, according to the model used in the SLIMMER software (1992). The subsequent grain growth once the recrystallization is completed is also incorporated by means of time dependent equations available in the literature (Siciliano et al., 1996). Finally, the numerical predictions determined with the proposed FV model are compared to the measured surface temperatures and rolling loads obtained from the hot strip rolling of a low Carbon-Manganese steel in a 7-stand finishing mill.

2. Mathematical modeling

2.1. Constitutive equations

In bulk metal forming such as the hot rolling process, the final material properties depend essentially upon the strain, strain-rate and temperature fields. Considering first the assumption of small elastic strains, the total strain rate tensor can be decomposed into an elastic part and a viscoplastic part :

$$\dot{\boldsymbol{\varepsilon}} = \dot{\boldsymbol{\varepsilon}}^{\mathbf{e}} + \dot{\boldsymbol{\varepsilon}}^{\mathbf{vp}} \tag{1}$$

Then, the elastic strains are usually very small in comparison to the plastic or viscoplastic strain levels in the hot rolling process and can, thus, be neglected. The total strain-rate can defined by means of the viscoplastic model of Perzyna together with the associated plastic flow rule (Soto et al., 1993) :

$$\dot{\boldsymbol{\varepsilon}} = \gamma \left\langle \phi(F) \right\rangle \frac{\partial F}{\partial \boldsymbol{\sigma}} \tag{2}$$

where γ is a fluidity parameter, F is the yield function, $\left\langle \phi(F) \right\rangle = 0$ when $F < 0$ and $= \phi(F)$ when $F \geq 0$ whereas $\boldsymbol{\sigma}$ is the Cauchy stress tensor. Assuming an isotropic material behavior, F can be defined by the von Mises yield surface defined by the following yield function :

$$\mathbf{F} = \sqrt{\frac{3}{2}\mathbf{S} : \mathbf{S}} - \bar{\sigma} \tag{3}$$

where $\mathbf{S}$ is the deviatoric stress tensor and $\bar{\sigma}$ is a scalar measure of the material flow-stress. On the other hand, the behavior of a linear isotropic Newtonian fluid relates the deviatoric stress and the total or viscoplastic strain-rate tensors through the viscosity μ, *i.e.* :

$$\mathbf{S} = 2\mu\, \dot{\boldsymbol{\varepsilon}} \tag{4}$$

Thus, the solution of the deformation process is attained by establishing an expression for the viscosity in Eq. (4). By introducing firstly the definition of the effective strain-rate conjugated of the von Mises effective stress, Eq. (3),

$$\dot{\bar{\varepsilon}} = \sqrt{\frac{2}{3}\dot{\boldsymbol{\varepsilon}} : \dot{\boldsymbol{\varepsilon}}} \tag{5}$$

and then assuming $\phi(F)$ as an exponential function $(F)^n$ and a viscoplastic loading stable condition of, i.e., $(F)^n > 0$, it is possible to obtain an expression for the viscosity by combining Eqs. (2-5) :

$$\mu = \frac{\bar{\sigma} + (\dot{\bar{\varepsilon}}/\gamma)^{1/n}}{3\dot{\bar{\varepsilon}}} \tag{6}$$

It should be noted that the particular case of ideal plasticity is obtained when $\gamma = \infty$ in Eq. (6), that is :

$$\mu = \frac{\bar{\sigma}}{3\dot{\bar{\varepsilon}}} \tag{7}$$

and that even so the viscosity nonlinearity can be accounted for through the flow stress definition $\bar{\sigma}$ which, in turn, may depend upon the accumulated effective strain $\bar{\varepsilon}$, the effective strain-rate $\dot{\bar{\varepsilon}}$, the temperature T and some internal or state variables v_k, *i.e.*,

$$\mu = \mu(\bar{\varepsilon}, \dot{\bar{\varepsilon}}, T, v_k) \tag{8}$$

Therefore, the material behavior in bulk metal forming processes can be considered as rigid-viscoplastic likewise the constitutive law of an incompressible non-Newtonian fluid (Zienkiewicz et al., 1978). Once the viscosity, Eq. (7), is calculated from the current fluid state, the stress components of the Cauchy tensor can be determined from the additive decomposition into a deviatoric part and volumetric part, that is,

$$\boldsymbol{\sigma} = \mathbf{S} - p\,\mathbf{I} = 2\mu\,\dot{\boldsymbol{\varepsilon}} - p\,\mathbf{I} \tag{9}$$

where – p is the hydrostatic pressure and $\mathbf{I}$ is the second order identity tensor. For the case small infinitesimal strains, the strain-rates can be obtained from the velocity field $\mathbf{v}$ by :

$$\dot{\boldsymbol{\varepsilon}} = \frac{1}{2}\left[\nabla \mathbf{v} + (\nabla \mathbf{v})^T \right] \tag{10}$$

2.2. Transport equations

The material behavior during the hot rolling process is highly coupled to the temperature and the strain-rate. Thus, the solution of the hot deformation is achieved by solving the temperature, velocity and pressure fields simultaneously. For a steady-state flow condition and assuming plastic incompressibility, the hot slab or strip motion and temperature are determined from the transport equations or balance laws for conservation of energy, momentum and mass. Hereafter, these equations are described in an Eulerian or spatial reference frame. Firstly, the temperature T is determined from the solution of the energy balance equation :

$$\nabla \cdot (\rho C_p \, \mathbf{v} T) = \nabla \cdot \left(\frac{K}{C_p} \nabla T \right) + S_T \tag{11}$$

where ρ , C_p and K are the material density, specific heat per unit volume and conductivity respectively which may depend upon the temperature. The source term S_T in Eq. (11) represents the rate of energy dissipation per unit volume resulting from the plastic deformation process and can be defined by :

$$S_T = \frac{\eta}{J} \int_V \boldsymbol{\sigma} : \dot{\boldsymbol{\varepsilon}} \, dV \tag{12}$$

where η is the fraction of the plastic work which is transformed into heat and J is the mechanical equivalent of heat. Then, the velocity **v** and the pressure p are determined from the solution of the conservation of momentum given by :

$$\nabla \cdot (\boldsymbol{\rho} \, \mathbf{v} \, \mathbf{v}) = \nabla \cdot \boldsymbol{\sigma} \tag{13}$$

together with the conservation of mass or continuity equation, that is :

$$\nabla \cdot (\rho \, \mathbf{v}) = 0 \tag{14}$$

It should be noted that Eq. (13) can be rewritten by introducing the Cauchy tensor, Eq. (9), as :

$$\nabla \cdot (\rho \, \mathbf{v} \, \mathbf{v}) = \nabla \cdot (\mu \nabla \cdot \mathbf{v}) - \nabla p + S_{\mathbf{v}} \tag{15}$$

where $S_{\mathbf{v}}$ are the remaining cross derivatives terms from $\nabla \cdot \boldsymbol{\sigma}$.

The transport equations, Eqs. (11-15) are discretized using the Finite Volume (FV) method for the 3D case of an arbitrary domain, *i.e.*, non-orthogonal, together with the "Body Fitted Coordinate" grid generation technique (Thompson et al., 1985).

2.3. Microstructure evolution

Figure 1 illustrates the behavior of a low carbon steel deformed at high temperatures, such as the hot rolling process, where the material work-hardening as well as restoration mechanisms of recovery and recrystallization can be observed. The restoration events are respectively denoted as dynamic and static depending whether they take place concomitantly or not with the stress loading. At the onset of the deformation process, the material work hardens due to the increase of the density of dislocations which, in turn, are arranged into subgrains boundaries. As the plastic strain level increases, the annihilation and generation rates of dislocations are counteracted producing, as a result, a steady-state flow-stress shown by the plateau (a) in Fig. 1. This restoration mechanism is known as dynamic recovery and its resulting microstructure, consisted of well-defined subgrains, is the source of the static recrystallization nuclei (Barbosa, 2002).

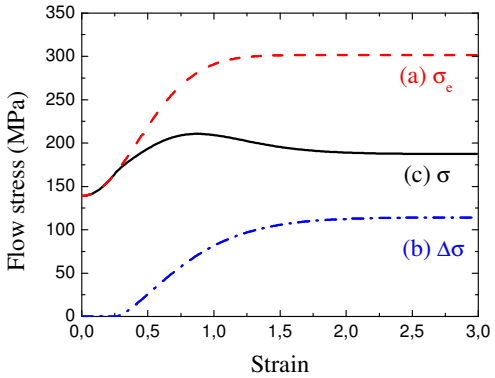

Figure 1. Low carbon flow stress-strain curve determined for an initial austenite grain size of 20 μm and constant values of the strain-rate (4.5 s^{-1}) and temperature (900^0 C) depicting the mechanisms of : (a) dynamic recovery (b) softening due to dynamic recrystallization and (c) the superposition of events (a) and (b) (Colás, 1996).

When the dynamic recovery is the only active restoration mechanism, the flow-stress can be described as (Beynon and Sellars, 1992) :

$$\sigma_e = \sigma_0 + (\sigma_{SS} - \sigma_0)\left[1 - exp(-C\varepsilon)^m\right] \tag{16}$$

where σ_0 is the stress at zero plastic strain, σ_{SS} is the steady-state flow-stress and m is the work-hardening exponent. C depends upon the Zener-Hollomon parameter defined as :

$$Z = \dot{\bar{\varepsilon}}\, exp\left(\frac{Q}{RT}\right) \tag{17}$$

where $\dot{\bar{\varepsilon}}$ is the effective strain-rate, Eq. (5), Q is the apparent activation energy for deformation, R is the gas constant (8.31 J/K mol) and T is the absolute temperature of deformation. Likewise, the flow stresses σ_0 and σ_{SS} depends upon the deformation conditions and can be generally defined as :

$$\sigma_{FS} = A_1\, sinh^{-1}\left(\frac{Z}{A_2}\right)^{A_3} \tag{18}$$

where A_n are material parameters determined from experimental data, for instance, from hot plane-strain compression or torsion tests.

On the other hand, when the recovery process is insufficient so as to decrease the activation energy of deformation, the multiplication of dislocations can produce the nucleation and growth of recrystallized grains during deformation. In this case, such as in austenite, the flow-stress curve raises up to a maximum value, the peak stress, accompanied by an additional softening reaching a steady-state value. The onset of dynamic recrystallization is characterized by a critical strain :

$$\varepsilon_c = a\,\varepsilon_p \tag{19}$$

which is estimated from the strain corresponding to the peak in the flow-stress given by :

$$\varepsilon_p = A\, d_0^{\,p}\; Z^q \tag{20}$$

where d_0 is the initial grain size whereas a, A, p and q are material parameters.

The softening due to the dynamic recrystallization, see curve (b) depicted in Fig. 1, can be accounted for as (Beynon and Sellars, 1992) :

$$\Delta\sigma = (\sigma_{SS} - \sigma'_{SS})\left\{1 - \exp\left[-k'\left(\frac{\bar{\varepsilon} - a\,\varepsilon_p}{\varepsilon_p}\right)^{m'}\right]\right\} \tag{21}$$

where σ'_{SS} is the current steady-state flow-stress at large strains, described in the form of Eq. (18), and k' and m' are material parameters. The curve (c) in Fig. 1 is obtained by superposing the effects of dynamic recovery and dynamic recrystallization, that is :

$$\text{If } \bar{\varepsilon} < \varepsilon_c \;\therefore\; \bar{\sigma} = \sigma_e \tag{22}$$

and

$$\text{If } \bar{\varepsilon} \geq \varepsilon_c \;\therefore\; \bar{\sigma} = \sigma_e - \Delta\sigma \tag{23}$$

It should be noted that for a general state of stress the conjugated effective strain, $\bar{\varepsilon}$, must be calculated from the deformation history. An appropriate procedure for determining the effective strain together with the FV method can be achieved from the definition of the material derivative in an Eulerian reference frame written in terms of the velocity field and its gradient as :

$$\dot{\bar{\varepsilon}} = \frac{D\bar{\varepsilon}}{Dt} = \frac{\partial\bar{\varepsilon}}{\partial t} + \mathbf{v}\cdot\nabla\bar{\varepsilon} \tag{24}$$

where the term referring to the time derivative vanishes for a steady-state flow. Therefore, Eq. (24) can be rewritten as a first-order linear, hyperbolic differential equation with a source term from which the effective strain is obtained, *i.e.* :

$$\rho\,\dot{\bar{\varepsilon}} = \nabla\cdot(\rho\,\mathbf{v}\,\bar{\varepsilon}) \tag{25}$$

The stored energy resulting from the deformation of dislocations also promote additional microstructure changes immediately upon unloading. These restoration mechanisms by static recovery or recrystallization can also be followed by grain growth if there is enough time between the deformation intervals, as is the case for plate and roughing mills. On the other hand, the hot strip or finishing process is characterized by decreasing time intervals and increasing and strain-rates per pass and may, therefore, lead to dynamic recrystallization followed by metadynamic recrystallization. The latter starts from the partly or steadily recrystallized structure from dynamic recrystallization after a deformation over the critical strain, Eq. (19), as discussed by Morgridge (2002). In order to take into account the partially recrystallized regions which may receive further deformation, the following correction for the effective strain is made :

$$\bar{\varepsilon} = \bar{\varepsilon}_N + (1 - X)\,\bar{\varepsilon}_{N-1} \tag{26}$$

where N is the current pass or stand. In Eq. (26), X is the static recrystallized volume fraction after the time t and is well described by the Avrami equation (Beynon and Sellars, 1992) :

$$X = 1 - \exp\left[- 0.693\,(t/t_{0.5})^k \right] \tag{27}$$

where $t_{0.5}$ is the time needed for half recrystallization. In plain Carbon-Manganese steels the exponent k is equal to 1.0 and 1.5 for static recrystallization and metadynamic recrystallization mechanisms respectively (Siciliano et al., 1996). In Eq. (27), the process time t is determined in the same manner as for the effective strain, see Eqs. (24-25).

The corresponding Carbon-Manganese times for half recrystallization and recrystallized grain sizes d for the events of static recrystallization (SRx) and metadynamic recrystallization (MDRx) can be predicted by the following equations (Siciliano et al., 1996) :

$$\text{If } \bar{\varepsilon} < \varepsilon_c \qquad \begin{aligned} t_{0.5}^{SRx} &= 2.3 \times 10^{-15}\, \bar{\varepsilon}^{-2.5}\, d_0^2 \exp\left(\frac{230{,}000}{RT} \right) \\ d^{SRx} &= 343\, \varepsilon^{-0.5}\, d_0^{0.4} \exp\left(- \frac{45{,}000}{RT} \right) \end{aligned} \tag{28}$$

$$\text{If } \bar{\varepsilon} \geq \varepsilon_c \qquad \begin{aligned} t_{0.5}^{MDRx} &= 1.1\, Z^{-0.8} \exp\left(\frac{230{,}000}{R\,T} \right) \\ d^{MDRx} &= 2.6 \times 10^4\, Z^{-0.23} \end{aligned} \tag{29}$$

Once recrystallization is completed, the austenite grain may continue to growth as a function of the available time between the deformation intervals. This further grain growth dependence upon the time for the hot strip rolling of Carbon-Manganese steels can be described by (Siciliano et al., 1996) :

$$\text{If } t_{ip} < 1\,s \qquad \begin{aligned} d^7 &= d_{SRx}^7 + 1.5 \times 10^{27} (t_{ip} - 4.32 t_{0.5}) \exp\left(- \frac{400{,}000}{RT} \right) \\ d^7 &= d_{MDRx}^7 + 8.2 \times 10^{25} (t_{ip} - 2.65 t_{0.5}) \exp\left(- \frac{400{,}000}{RT} \right) \end{aligned} \tag{30}$$

$$\text{If } t_{ip} > 1\,s \qquad \begin{aligned} d^2 &= d_{SRx}^2 + 4.0 \times 10^7 (t_{ip} - 4.32 t_{0.5}) \exp\left(- \frac{113{,}000}{RT} \right) \\ d^2 &= d_{MDRx}^2 + 1.2 \times 10^7 (t_{ip} - 2.65 t_{0.5}) \exp\left(- \frac{113{,}000}{RT} \right) \end{aligned} \tag{31}$$

where t_{ip} is the interpass time.

3. FV model

Figure 2 shows in a Cartesian coordinate system X_i (i = 1,2,3) the typical finite-volume mesh adopted in the numerical simulations of the hot strip rolling process. Due to the symmetry, only the half strip thickness is considered. The boundary conditions are described as follows.

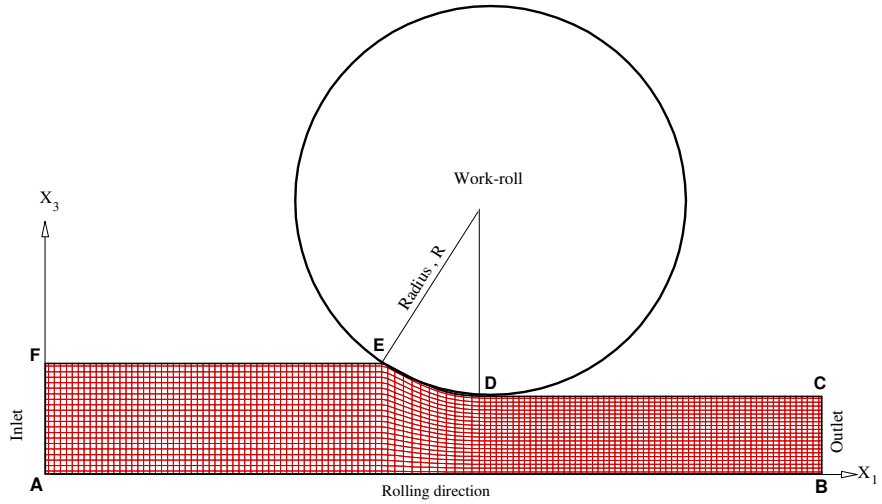

Figure 2. FV model of the hot strip rolling process.

At the surfaces E-F and C-D, before and after the deformation zone, the dominant heat transfer mechanisms are convection and radiation described by :

$$-K\left(\frac{\partial T}{\partial X_3}\right) = h\,(T - T_\infty) + \sigma\varepsilon\,(T^4 - T_\infty^4) \tag{32}$$

where T_∞ is the surrounding temperature, σ is the Stephan-Boltzmann constant whereas the convection heat transfer coefficient h and the emissivity factor ε has been taken equal to 12,500 W/m^2 K and 0.8 respectively. In the roll-gap, that is, at the contact region D-E between the strip and the work-roll, heat transfer is mainly by conduction :

$$-K\left(\frac{\partial T}{\partial \boldsymbol{n}}\right) = h_{con}\,(T - T_{WR}) \tag{33}$$

where $\boldsymbol{n}$ stands for the normal direction vector along the arc contact, h_{con} is the roll-gap heat transfer coefficient and T_{WR} is the work-roll temperature. At the symmetry plane A-B there is no heat flux along the normal direction X_3, i.e. :

$$\frac{\partial T}{\partial X_3} = 0 \tag{34}$$

as well as for the outlet section B-C along the normal direction X_1. The inlet temperature and the velocity field at the inlet section F-A first stand are assumed to be constant whereas the corresponding values at the outlet section B-C are computed from the transport equations described in § 2.2.

4. Material and finishing mill data

The material analyzed has been processed at the CSN steel plant and corresponds to a Carbon-Manganese steel for which the typical chemical composition is shown in Tab. 1. The plate thickness is equal to 35.4 mm with an average surface temperature of 984.7 ^{0}C and is reduced to 3.90 mm in a 7-stand finishing mill. The strip surface temperatures before and after each stand were measured with the help of an optical pyrometer as described elsewhere (Silva, 1997).

Table1. CSN C-Mn steel chemical composition (% of weight)

C	Mn	P	S	Al	Si	N	Nb
0.03	0.25	0.02	0.025	0.025	0.025	0.007	0.005

Table 2 shows the constitutive parameters describing the typical behavior of C-Mn steels during hot strip rolling, Eqs. (16-21), have been taken as the values available in the material database of the commercial software SLIMMER (Sheffield Leicester Integrated Model for Microstructural Evolution in Rolling). The initial austenite grain size d_0 at the first stand was assumed to be equal to 200 μm. The apparent activation energy for deformation Q, see Eq. (17) for the Zener-Hollomon parameter, has been taken equal to 300 kJ/mol whereas the parameter C in Eq. (16) was defined as :

$$C = 10\left[\,(\sigma_{01} - \sigma_0)\Big/(\sigma_{SS} - \sigma_0)\,\right]^2 \tag{35}$$

Table2. Constitutive material data for C-Mn steels (SLIMMER, 1992).

	σ_0			σ_{SS}			σ_{01}	
A_1	A_2	A_3	A_4	A_5	A_6	A_7	A_8	A_9
103.84	4.92×10^{13}	0.13	103.41	1.77×10^{11}	0.217	89.29	2.55×10^{11}	0.182
	σ'_{SS}			$\Delta\sigma$			ε_p	
A_{11}	A_{12}	A_{13}	k'	m'	a	A	p	q
106.72	3.88×10^{12}	0.146	0.49	1.4	0.7	5.6×10^{-4}	0.3	0.17

Table 3 presents the CSN 7-stand finishing mill data and the adopted values for the roll-gap heat transfer coefficient at each stand where the work-roll temperature T_{WR} is assumed to be constant and equal to 200 ^{0}C.

Table 3. CSN 7-stand finishing mill and heat transfer data.

Stand	1	2	3	4	5	6	7
Work-roll diameter (mm)	732	732	712	687	717	732	717
Initial thickness (mm)	35.40	24.80	17.13	11.68	8.37	6.12	4.70
Thickness reduction (%)	30.0	30.9	31.8	28.4	26.8	23.2	15.2
h_{con} (W/m^2 K)	5,000	6,000	8,400	9,500	12,100	15,500	16,700

5. Numerical results

Figure 3 shows the predicted temperature distribution determined for the first stand where a temperature increase is observed near to the strip central region up to the exit due to the conduction heat and generation from the plastic-work. The temperature and tangential velocity obtained at the slab surface along the rolling direction are shown in Fig. 4a. First the temperature decreases up to the contact with the work-roll and then reheats towards the stand exit section. As one could expect, the tangential velocity rises gradually within the contact zone due to the conservation of mass.

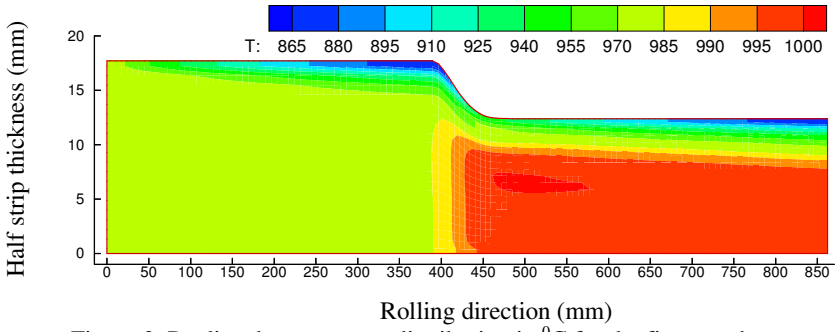

Figure 3. Predicted temperature distribution in ^{0}C for the first stand.

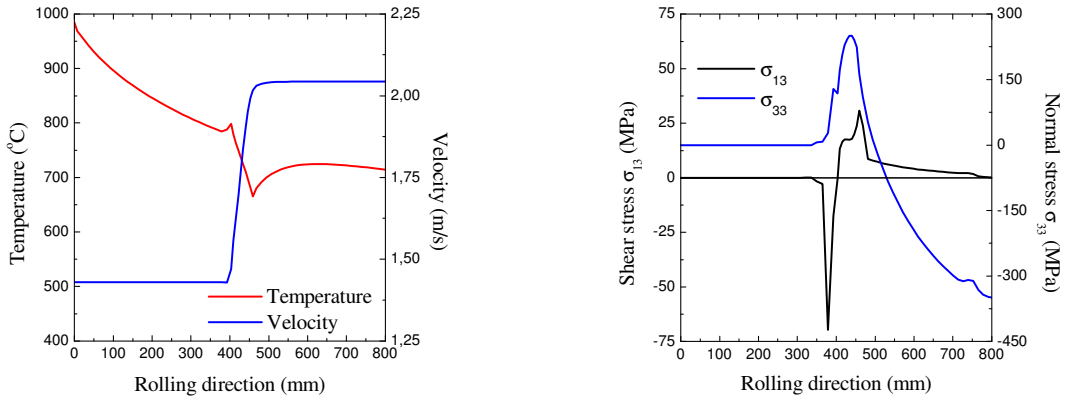

Figure 4. Numerically predicted distributions along the outer surface strip of (a) the temperature and tangential velocity and (b) the normal and shear stress determined for the first stand.

Even though neither the work-roll nor the contact friction are not taken into account in the present FV modeling, it is possible to note from Fig. 4b a change in the shear stress sign along the contact surface. This result is in agreement with the idea of a non-slip zone in the flat rolling process wherein the frictional contact forces are counteracted and from which the strip tangential velocity is greater than the work-roll velocity.

Table 4 compares the numerical predictions with the measured rolling loads and surface temperatures obtained from the 7-stand strip rolling of a C-Mn steel. The proposed model provides a better prediction for the rolling loads than to the average exit surface temperatures. Actually, the rolling loads predictions are extremely dependent upon the roll-gap heat transfer coefficient which has been adjusted so as to match the experimental loads. This table also shows the computed average austenite grain size resulting from metadynamic recrystallization determined at the outlet section. The range of the predicted grain sizes are in agreement with the expected grain refinement during the hot strip rolling process and with the numerical results obtained by the model proposed by Siciliano et al. (1996).

Table 4. Comparison between numerical predictions and experimental hot-strip mill data.

Stand	1	2	3	4	5	6	7
Measured rolling load (MN)	12.69	13.07	13.40	10.65	10.50	9.09	5.79
Predicted rolling load (MN)	12.65	12.98	13.31	10.56	10.40	8.97	5.78
Rolling load error (%)	0.31	0.68	0.67	0.80	0.90	1.30	0.17
Measured temperature (^{0}C)	876.8	891.6	876.7	904.9	925.1	903.1	911.0
Predicted temperature (^{0}C)	954.3	852.4	847.2	842.3	859.4	877.4	814.5
Temperature error (%)	8.8	4.3	4.2	9.9	7.1	2.8	5.0
Austenite grain size d (μm)	46	30	25	20	25	10	12

4. Concluding remarks

In this work, the finishing of a low C-Mn steel is analyzed with the help of a Finite-Volume (FV) model wherein the typical microstructural changes during the hot strip rolling process are taken into account. In the proposed model, the initial conditions at the inlet section, see Fig. 2, are the measured temperature at the slab surface and the velocity along the rolling direction for the first stand. Then, the corresponding predicted outlet temperature and velocity fields are prescribed as the initial conditions for the second stand and this procedure is repeated up to the last finishing stand. It is shown that the predicted rolling loads and temperatures are in good agreement with the measured data. However, these predictions are highly dependent upon the roll-gap heat transfer coefficients which, in turn, have been adjusted to match the experimental rolling loads. The typical grain refinement in the hot strip finishing has also been predicted.

5. Acknowledgements

The authors would like to acknowledge the research grants from CNPq (LPM, JAC and RB) and FAPERJ (LPM).

6. References

Barbosa, R., 2002, “Desenvolvimento e Perspectivas da Pesquisa em Metalurgia Física Aplicada à Laminação a Quente de Aços”, Aços : Perspectivas para os próximos 10 anos, Rede Aços, Ivani Bott (Ed.), 2002, Rio de Janeiro, pp. 11-22.

Beynon, J. H. and Sellars, C. M., 1992, “Modelling Microstructure and Its Effects During Multipass Hot Rolling”, The Iron and Steel Institute of Japan, Vol. 32, No. 3, pp. 359-367.

Colás, R., 1996, “A Model for the Hot Deformation of Low-Carbon Steel”, Journal of Materials Processing Technology, Vol. 62, pp. 180-184.

Morgridge, A. R., 2002, “Metadynamic Recrystallization in C Steels”, Bullet. of Mater. Science, Indian Acad. of Sc., Vol. 25, No. 4, pp. 291-299.

Siciliano Jr., F., Minami, K., Maccagno, T. M. and Jonas, J. J., 1996, “Mathematical Modeling of the Mean Flow Stress, Fractional Softening and Grain Size During the Hot Strip Rolling of C-Mn Steels”, The Iron and Steel Institute of Japan, Vol. 36, No. 12, pp. 1500-1506.

Silva, M. A. C., 1997, “Modelamento Matemático, Simulação Numérica e Validação do Processo de Laminação a Quente para Aços Baixo Carbono, Master Thesis, Universidade Federal Fluminense, Niterói, Rio de Janeiro, Brazil.

SLIMMER for Windows, 1992, Sheffield Leicester Integrated Model for Microstructural Evolution in Rolling, Pro Technology, University of Leicester, Leicester, United of Kingdom.

Soto, O., Oñate, E. and Codina, R., 1993, “Finite Element Analysis of Hot Rolling Processes”, Publicación CIMNE N. 40, Centro Internacional de Métodos Numéricos en Ingeniería, Spain.

Thompson, J. F., Warsi, Z. U. A. and Mastin, C.W., 1985, “Numerical Grid Generation”, North Holland, New York, Appendix C-3, p. 454.

Zienkiewicz, O.C., Jain, P.C. and Oñate, E., 1978, “Flow of Solids During Forming and Extrusion : Some Aspects of Numerical Solutions”, International Journal of Solids and Structures, Vol. 14, N. 1, pp. 15-38.

7. Responsibility notice

The authors are the only responsible for the printed material included in this paper.